Available online at www.sciencedirect.com
ScienceDirect
Acta Materialia 59 (2011) 2491–2500
Acta MATERIALIA
www.elsevier.com/locate/actamat

Driving force and growth mechanism for spontaneous oxide nanowire formation during the thermal oxidation of metals

Lu Yuan [a], Yiqian Wang [b], Rediola Mema [a], Guangwen Zhou [a,*]

[a] Department of Mechanical Engineering & Multidisciplinary Program in Materials Science and Engineering, State University of New York, Binghamton, NY 13902, USA

[b] The Cultivation Base for State Key Laboratory, Qingdao University, Qingdao 266071, People's Republic of China

Received 18 October 2010; received in revised form 24 December 2010; accepted 27 December 2010
Available online 1 February 2011

Abstract

The spontaneous formation of oxide nanowires (and whiskers) from the oxidation of metals is a well-established phenomenon that has, however, long resisted interpretation. Here we report new fundamental insights into this phenomenon by studying CuO nanowire formation during the thermal oxidation of copper. It is shown that the volume change associated with the solid-state transformation at the CuO/Cu_2O interface produces compressive stresses, which stimulate CuO nanowire growth to accompany the interface reaction. A kinetic model based on the stress-driven grain-boundary diffusion followed by rapid surface diffusion of cations on the sidewall of nanowires is developed to account for CuO nanowire growth. The mechanism proposed explains our observations on CuO nanowires and other past observations.

Keywords: CuO; Cu; Nanowires; Oxidation; Stress

1. Introduction

Formation of one-dimensional metal oxide nanowires (NWs) or whiskers has been intensively investigated because of wide technological applications and the intrinsic interest in structures with reduced dimensions. More recently, considerable attention has been directed to oxide NW formation by thermal oxidation of metals in oxygen atmosphere [1–9], largely due to its technical simplicity and large-scale growth capability. Oxide whisker growth from the oxidation of metals was first observed back in the 1950s [10,11] and since then numerous observations have been performed but have led to different theories regarding the mechanisms for the spontaneous oxide NW formation. Some are based on evaporation and condensation mechanism, i.e., vapor–solid (VS) model [8,12,13], or short-circuit diffusion up the center of the NWs [14–18]. Other work suggested that growth of oxide NWs occurs as a result of the accumulation and relaxation of compressive stresses in the oxidation processes [19–21]. Unclear to date, however, is the origin of the compressive stresses in the oxide layer and how they result in oxide NW growth.

The phenomenon of oxide NW formation from the oxidation of metals is not tied up with a single metal system but the oxidation of copper remains the most representative one [17,19–25]. It was proposed that the driving force for CuO whisker formation during the oxidation of copper is related to the high compressive stress in the oxide layer resulting from the large difference in the molar volumes of the metal and oxides [17,26,27]. Since both Cu_2O and CuO are cation-deficient p-type oxides, it has been shown univocally that the oxide growth is controlled via outward diffusion of cations during the oxidation of Cu [15,17,28–32]. The new oxide formation occurs at the gas/oxide interface so that the oxide layer grows preferentially into free space. Such unconstrained growth would not be expected to develop stress (the effect of epitaxial stress is limited to the first

* Corresponding author.
E-mail address: gzhou@binghamton.edu (G. Zhou).

1359-6454/$36.00 © 2010 Acta Materialia Inc. Published by Elsevier Ltd. All rights reserved.
doi:10.1016/j.actamat.2010.12.052

~50 nm of oxide and is not applicable to oxide NW formation, which requires the first growth of macro-thick surface oxide layers) [28].

Some unique experiments have been performed and suggested that CuO NWs grow from the tip and are not extruded from the base oxide layers during the oxidation of Cu substrates [17,33]. For such a process, the NW growth must call for transport of Cu ions from the base to growth tip. It was suggested that oxide NWs or whiskers grow predominately by surface diffusion of metal species from the NW base to top along a tunnel centered on the core of a screw dislocation [14–18]. However, such a scenario contradicts with many recent experimental observations, which reveal that oxide NWs have a bicrystal or single crystal structure (i.e., no hollow pipe present along the axial core of NWs) [6,8,20,23,33]. Therefore, it is paramount to identify the driving force leading to the initiation of oxide NW formation and the mass transport mechanisms governing the one-dimensional NW growth. In this work we choose to study CuO NW formation during the oxidation of copper as a model system to understand the mechanism of oxidation-induced oxide NW growth. Meanwhile, our interest in this system also stems from the prospective broad applications of nanostructured CuO. A number of interesting properties have been found in this p-type semiconductor material that have led to its myriad technological applications in important fields including solar energy conversion [34,35], photocatalysts [36], fuel cells [37,38], emission control [39–41], cathode materials in lithium ion batteries [42], gas sensing [6,9,43], and heterogeneous catalysis for hydrocarbons conversion reactions [44,45].

2. Experimental details

High-purity copper substrates (99.99% purity) are first cleaned in aqueous 1.0 M HCl solution to remove the native oxide layer and then thoroughly rinsed with deionized water followed by ultrasonication in acetone for 5 min. The cleaned Cu substrates are then put on a substrate heater in the vacuum chamber, where the base pressure is $\sim 2 \times 10^{-6}$ torr and the sample temperature is monitored using a K-type thermocouple in contact with the sample heater. Prior to the oxidation reaction, the Cu substrate is annealed at 600 °C under 200 torr pressure Ar–10% H_2 pressure for 2 h to further remove any residual native oxide as well as to improve the surface flatness. After the annealed Cu substrate is cooled down to room temperature (cooling rate: ~10 °C min^{-1}) under the H_2 gas, the chamber is pumped to vacuum ($\sim 2 \times 10^{-6}$ torr), and then filled with 200 torr oxygen pressure (the purity of oxygen is 99.999%). The chamber is then sealed and the annealed Cu sample is heated to the desired temperature (350 °C or 450 °C) at 20 °C min^{-1} in the oxygen gas. After the Cu sample is oxidized for different durations (from 30 min to 4 h), it is cooled down in the same oxygen atmosphere to room temperature at the rate of ~10 °C min^{-1}. Surface morphology and chemical composition of the oxidized samples are examined using a field emission scanning electron microscope (FEG-SEM) FEI Supra 55VP. Length and diameter of CuO nanowires are measured from SEM images. The morphology and microstructure of individual CuO NWs are analyzed by transmission electron microscopy (TEM) using a JEOL 2100F operated at 200 kV.

3. Experimental results

Optically the surface of the Cu substrate turns black in color after the oxidation treatment, suggesting that the surface oxide is CuO, which is known to be black in color. Examination by SEM indicates the formation of oxide NWs over the entire surface. Fig. 1 is an SEM image of the Cu substrate oxidized at 450 °C for 2 h. It can be seen that the surface is covered by dense CuO NWs, with diameters ranging from 50 to 100 nm and lengths up to tens of microns. The oxide NWs are relatively aligned and perpendicular to the substrate surface. Most NWs have uniform diameter along their longitudinal axial direction and the NW surface is smooth and highly faceted, as shown by the magnified view of the inset SEM image in Fig. 1, where the facets of the NW surfaces belong to $(2\,0\,\bar{2})$ and $(\bar{2}\,0\,2)$-type planes.

Fig. 2a is a cross-sectional SEM image of an oxidized Cu sample, from which a three-layered structure can be identified: a ~3-μm-thick bottom layer that lies directly above the Cu substrate, an intermediate thin layer with a thickness of about ~600 nm, and a top oxide NW layer. Using X-ray energy dispersive spectroscopy (EDS) analysis, these different layers can be easily identified as Cu_2O and CuO with Cu_2O being the bottom layer and CuO being the intermediate and top layers. Fig. 2b is a magnified view from the interface area between the intermediate CuO layer and the top layer of CuO NWs. All the CuO NWs appear to grow directly on the grains of the intermediate CuO layer. SEM examination also indicates that some weak correlation exists between the NW diameter and the lateral size of the grains on which NW growth occurs, i.e., CuO

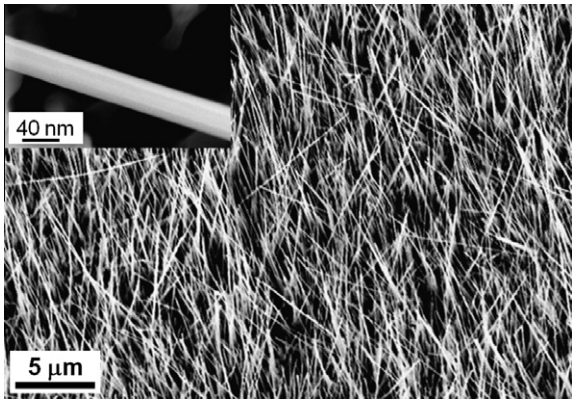

Fig. 1. SEM micrograph of the surface morphology of a Cu substrate oxidized at 450 °C for 2 h. Inset: magnified SEM view of a single CuO NW.

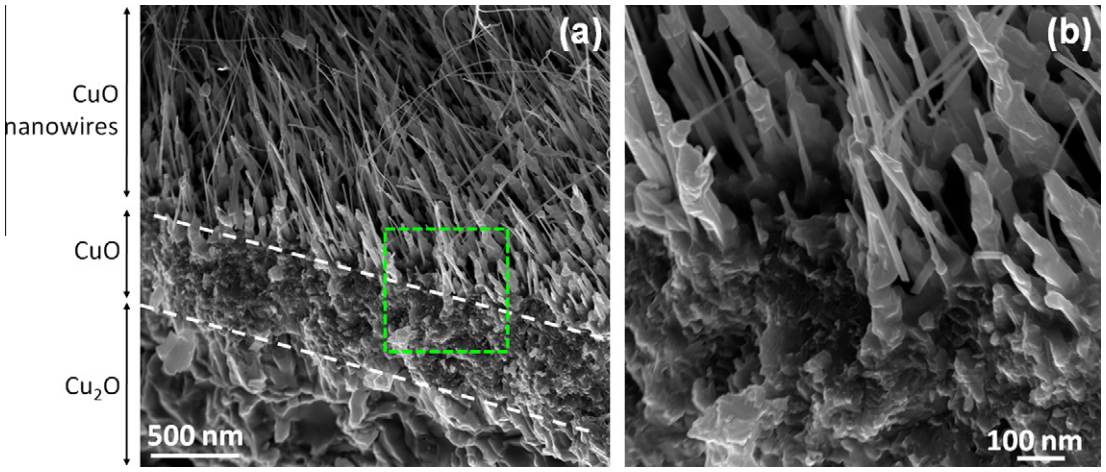

Fig. 2. (a) Cross-sectional SEM image of a Cu substrate oxidized at 450 °C for 2 h, showing the Cu_2O and CuO layers and the growth of CuO NWs on the CuO layer; (b) magnified view from the NW root region marked by the dashed square.

NWs with a larger diameter are associated with larger grains. It is also noted that some short NWs have a tapered shape, with the maximum diameter at the base. An intriguing feature is that tapered NWs have a much rougher side surface in comparison with long and uniform diameter NWs.

To further confirm that CuO NWs originate directly from individual CuO grains rather than from grain boundaries (GBs), the Cu substrate is oxidized for a short duration so that their initial growth morphology can be observed. As illustrated in Fig. 3, the oxide surface consists of highly faceted CuO grains and NWs are formed directly on top of the grains. In contrast, the oxide layer on the grain boundary (GB) regions hardly shows any signatures of formation of NWs. One very instructive comparison comes from the occurrence of tin whisker growth on tin plated Cu lead frames, where whiskers are extruded from the GBs and the cross-sectional shape of whiskers is determined by the GB geometry at the surface [46]. As revealed in Fig. 3, the cross-sectional shapes of CuO NWs show no correlation with the GB geometry, confirming that the NW formation is not driven by a GB extrusion process.

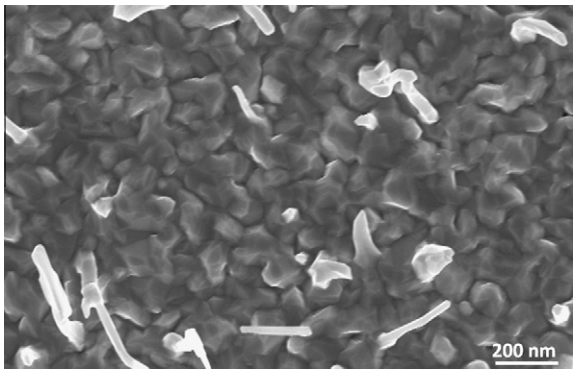

Fig. 3. SEM micrograph of a Cu substrate oxidized at 450 °C for ~30 min, showing the initial growth morphology of CuO NWs.

Since CuO NWs are formed directly on the intermediate CuO layer which grows on the inner Cu_2O layer, growth behaviors of the Cu_2O and CuO layers would provide insight into the interplay of the two oxide layers during the NW growth. We measured the thickness of the CuO and Cu_2O layers on Cu substrates oxidized for different oxidation times. Fig. 4a and b shows cross-sectional SEM images of the Cu substrates oxidized at 450 °C for 30 min and 3 h, respectively. For both samples, the oxides consist of two condense oxide layers, i.e., the inner Cu_2O layer and the intermediate CuO layer. The Cu_2O layer is much thicker than the CuO layer. The Cu_2O layer is composed of coarse columnar grains perpendicular to the Cu base whereas the intermediate CuO layer consists of considerably fine grains.

For oxidation controlled by outward diffusion of metal cations, oxide growth should follow the parabolic growth law, i.e., $x \sim (2kt)^{1/2}$, where x is the thickness of the oxide layer, k the rate constant, and t the oxidation time. A parabolic plot of the oxide layer thickness thus yields a straight line. Fig. 4c shows the measured thickness of the two oxide layers of Cu_2O and CuO for oxidation time varying from 30 min to 4 h. As can be seen, the parabolic plots yield straight lines for the growth of the two oxide layers, suggesting that their growth is controlled by outward diffusion of Cu cations through the Cu_2O and CuO layers. According to the previous work [29,30,32], the rate-limiting step for the oxidation of Cu in the intermediate temperature range (<500 °C) is GB diffusion, which is essentially parabolic.

The crystalline nature and microstructure of the oxide NWs is also examined using TEM and selected-area electron diffraction (SAED). A typical bright-field (BF) TEM image of an individual CuO NW is shown in Fig. 5a, which reveals clearly that the NW is divided by a twin boundary along its length direction. Fig. 5b displays a high-resolution TEM (HRTEM) image, which shows that the NW has a bicrystalline structure and there is no hollow pipe along

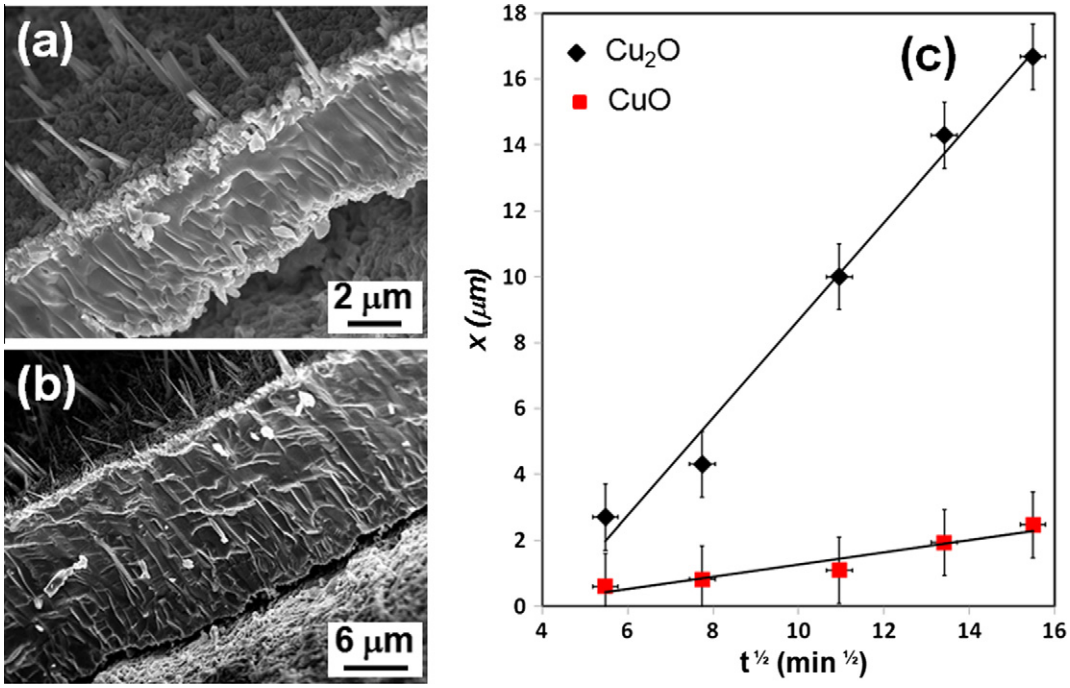

Fig. 4. (a and b) Cross-sectional SEM images showing the CuO and Cu_2O layers on Cu substrates oxidized at 450 °C for 30 min and 3 h, respectively; (c) thickness of the two oxide layers vs. the square root of the oxidation time, where the oxide thickness is plotted vs. square root of oxidation time.

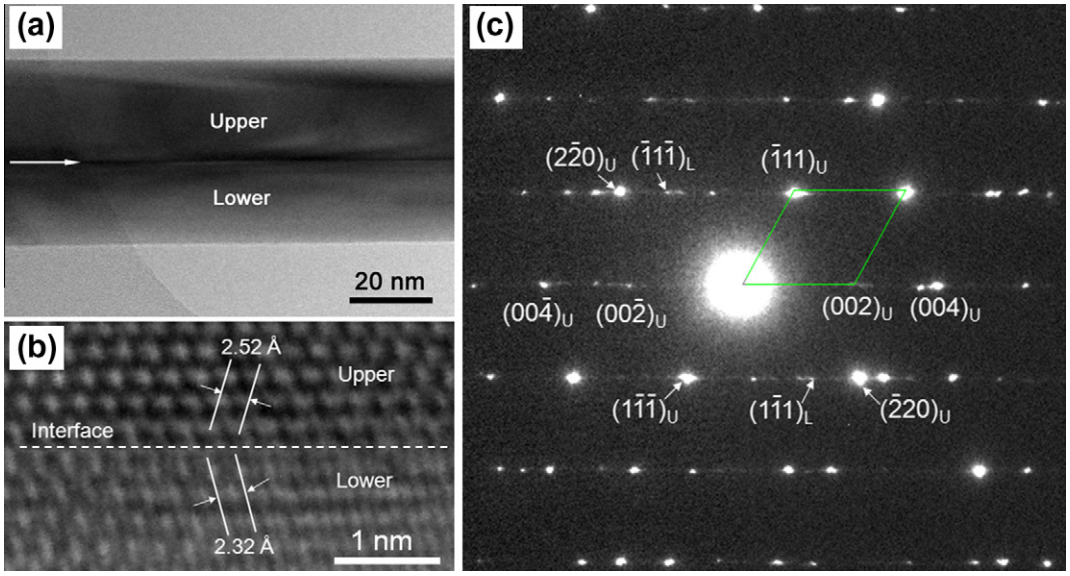

Fig. 5. (a) The contrast from a BF TEM image of an individual CuO NW suggests the presence of a twin boundary along the axial direction of the NW. (b) HRTEM image of the NW showing the twin boundary of the NW. (c) SAED pattern obtained from a single NW. Indices with subscript L refer to the lower side of the NW shown in (a and b); indices with subscript U refer to the upper side.

the core of the NW. Each side of the NW is single crystal with well-defined crystal lattice planes. The interplanar spacings of each side as measured from the HRTEM image are 2.52 Å and 2.32 Å, respectively, corresponding well with the calculated spacings of $(\bar{1}\,1\,1)$ and $(1\,\bar{1}\,1)$ planes of monoclinic CuO ($a = 4.69$ Å, $b = 3.42$ Å, $c = 5.13$ Å, and $\beta = 99.55°$). TEM examination of different CuO NWs indicates that twin boundary is a common structure feature for most NWs, while the exact locations of the twin boundary within the NWs may vary for different NWs. Fig. 5c shows a typical SAED pattern obtained from a single CuO NW, where the zone axis is along [1 1 0] direction. The diffraction pattern can be identified as consisting of two sets of diffraction spots with mirror symmetry, consistent with the nature of the bicrystalline structure within the nanowire.

4. Discussion

NW growth is usually described by either vapor–solid (VS) or vapor–liquid–solid (VLS) mechanisms [1,47]. During the oxidation of Cu substrates, CuO NW formation occurs at relatively low temperatures (significantly lower than the melting points of both Cu and its oxides) and at negligibly small equilibrium vapor pressures of the pure metal or its oxides and therefore cannot be ascribed to any of these mechanisms. In analogy to Sn whisker growth driven by the compressive stresses accumulated within the underlying Sn layer, oxide NW growth during metal oxidation has also been explained by the stress-driven mechanism [19,20,23,27]. However, it remains unclear how the compressive stress is generated in the oxide layers in view of the unconstrained oxide growth on the free surface by outward diffusion of Cu cations. Here it is proposed that the CuO NW formation is related to the CuO/Cu_2O interface reaction, which produces compressive stresses in the CuO layer and thus drives outward diffusion of Cu cations along CuO GBs, resulting in CuO NW growth on CuO grains.

Copper forms two thermodynamically stable oxides, CuO and Cu_2O, on the reaction with oxygen. The oxide scale consists of Cu_2O and CuO with CuO being the topmost layer, as revealed in Figs. 2 and 4. To incorporate gas oxygen into the oxide lattice for the oxide growth, the oxygen first chemisorbs on the CuO surface by attracting an electron from a Cu lattice site, thus forming an electron hole. The chemisorbed oxygen is fully ionized forming another hole and a Cu^{2+} ion enters the surface to partner the O^{2-}, thus forming another hole and a vacancy in the cation sub-lattice. Therefore, Cu cation vacancies and electron holes are created at the CuO/oxygen interface and this occurs when O_2 at the CuO surface utilizes Cu^{2+} ions from the outer CuO lattice to form new CuO molecules, in accordance with the reaction [48]

$$\frac{1}{2}O_2 \leftrightarrow CuO + 2h^+ + V_{Cu}^{-2} \quad (1)$$

where h^+ represents an electron hole having an effective charge +e and V_{Cu}^{-2} represents a cation vacancy having an effective negative charge of −2e. The cation vacancies and electron holes so produced migrate through the CuO and Cu_2O layers, being annihilated finally at the Cu_2O/Cu interface. Similarly, the phase-boundary reaction at the Cu_2O/CuO interface during growth of the Cu_2O layer also generates new cation vacancies and electron holes, which migrate through the Cu_2O layer and are annihilated at the parent metal of Cu. These defect species originate in the solid-state reaction in which the oxygen-richer layer (i.e. CuO layer) undergoes decomposition to form more oxide of the Cu_2O layer at the Cu_2O/CuO interface in accordance with the reaction

$$CuO \leftrightarrow Cu_2O + h^+ + V_{Cu}^{-1} \quad (2)$$

where V_{Cu}^{-1} represents a cation vacancy in Cu_2O layer. That is, a cation vacancy, together with an electron hole h^+, is produced by the solid-state transformation of one molecule of CuO to form one new Cu_2O for increasing the thickness of the Cu_2O layer, i.e., growth of the Cu_2O layer requires decomposition of the oxygen-richer CuO layer to obtain the necessary oxygen. All cation vacancies generated in the reactions given by Eqs. (1) and (2) eventually flow to the parent Cu for annihilation, accompanied by an equivalent outward flow of cations. The parabolic growth of both the Cu_2O and CuO layers (Fig. 5c) suggests that the oxidation is diffusion-controlled, i.e., the CuO decomposition at the CuO/Cu_2O interface is faster than the diffusion rates of Cu cations in the two oxide layers. According to the previous studies [49,50], the diffusivity of Cu cations in CuO is smaller than that in Cu_2O. This explains why the Cu_2O layer is much thicker than the CuO layer.

Cu_2O grows at the expense of CuO via the continuous oxide-forming reaction at the interface between the two oxide layers. Since the two oxides have different molar volumes (the cell volumes of Cu_2O and CuO are 77.83 $Å^3$ and 81.16 $Å^3$, respectively), they both grow by outward diffusion of cations. The ensuring difficulties in local volume accommodation give way to the generation of stresses at the Cu_2O/CuO interface region, which would serve as the driving force for outward diffusion of Cu atoms, in addition to the normal Cu cation diffusion flux driven by the chemical potential gradient established by the many-orders-of-magnitude difference in oxygen partial pressure between the oxide–atmosphere and oxide–metal interfaces. For this particular case, compressive stresses are accumulated in the CuO interface region due to the volume shrinkage associated with the conversion of CuO into Cu_2O. The CuO upper layer is believed to provide a path to release the stress. This is because the CuO layer is much thinner than the inner Cu_2O layer, in addition to the fine grain size and the large number of GBs present in the CuO layer (Figs. 2 and 4). Our observations indicate that the thickness of the CuO layer for the initiation of CuO NW growth is about 1 μm or less. This can be attributed to the driving force for the oxide NW formation, which requires effective relaxation of the compressive stresses at the CuO/Cu_2O interface via GB diffusion and thus sets the thickness limit for the CuO layer.

For the intermediate range of the oxidation temperature (~300–550 °C) under which oxide NW growth occurs and the small size of grains in the CuO layer, the atomic flux comes primarily along CuO GBs. Cu ions diffuse along GBs from the region in compression (i.e., near the CuO/Cu_2O interface) to the outer surface of the CuO layer, which is stress-free. This diffusion is driven by the gradient of the chemical potential induced by the gradient of the stress, σ, acting along each GB. The chemical potential in the GB plane is related to the stress, σ, by the relation $\mu = \mu_0 - \sigma\Omega$, where μ_0 is the chemical potential of an atom in a stress-free system and Ω is the atomic volume. From Fick's law, the diffusive flux along a given GB depends

on the gradient of the normal-stress component, σ_n, along the GB as follows [51]:

$$J_{GB} = \frac{D_{GB}\delta\Omega}{kT}\frac{\partial\sigma_n}{\partial s} \quad (3)$$

Here D_{GB} is the GB diffusion coefficient, δ the GB width, k Boltzmann's constant, T the absolute temperature, and s is the local spatial coordinate along the diffusion path. As revealed in Fig. 3, existing CuO grains serve as the structure template for initiating CuO NW growth, i.e., Cu cations diffusing along the GBs are deposited on the top of grains via surface diffusion. The surface diffusion is driven by the concentration gradients of Cu ions between the GB junction area and the NW root and the NW tip, where Cu ions are incorporated into the NW growth by reacting with vapor oxygen. The diffusion of Cu cations to support the growth of an oxide NW follows the paths shown schematically in Fig. 6. Such a process of incorporating Cu atoms onto exiting CuO grains is kinetically more favorable than forming new CuO nuclei at the GB junction area since it not only has to overcome a nucleation barrier but also blocks the diffusion path of Cu ions along the GB. As long as the compressive stress in the CuO layer is maintained by the solid-state phase transformation at the Cu_2O/CuO interface, this outward diffusion flux of Cu atoms continues and acts as a continual source of Cu cations for CuO NW growth.

The above growth process requires the presence of atomic steps at the NW tip as a sink for incorporation of arriving Cu ions and oxygen atoms directly from the vapor. NWs are observed to have a bicrystal structure, where a large part of the atoms on the tip are at kink or step positions near the twin boundary if the bicrystal boundary is continued through the NW and to the NW tip. This is indeed the case, as revealed by the HRTEM image obtained from a typical CuO NW tip (Fig. 7a and b). The atomic steps around the tip provide sites for easy attachment for arriving Cu cations. On the other hand, the sidewalls of long CuO NWs with uniform diameter have smooth surfaces (Fig. 7c), for which the incorporation of Cu ions onto the side surface is kinetically suppressed due to the lack of growing places (kinks) on the surface.

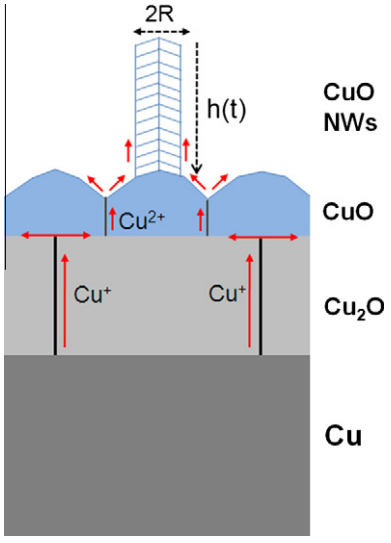

Fig. 6. Mass transport mechanisms of Cu^{2+} ions for CuO NW growth: Cu ions diffuse outward from the CuO/Cu_2O interface to the free surface via GB diffusion driven by the CuO/Cu_2O interfacial strain, followed by surface diffusion from GB junction areas to the NW root and then to the NW tip driven by the concentration gradient.

A pertinent question is how bicrystal (or twin) boundaries are generated in the NWs. A useful analogy is the formation process of screw dislocation in whiskers, where a threading dislocation at the surface was suggested to serve as the whisker nucleation point and the dislocation would be continued into the whisker [17,52]. By the same token, the formation of twin boundaries can originate from the multifacets of CuO grains. As revealed in Fig. 3, CuO grains are highly faceted and each facet would serve as a template for NW growth. The NW growth starts from facet corners where steps and kinks are rich, and then spreads over faceted surfaces of the grain. Therefore, the crystals grown on each facet are naturally joined together to form a twin or multi-twin structure started from the grain top and continued into the NW along the axial direction. The formation process of twin boundaries created by this mechanism is schematically shown in Fig. 6. Cu cations supplied from the GB diffusion can diffuse naturally onto the sidewall of NWs via substrate–NW adatom exchange to sustain the unidirectional growth.

The growth kinetics of NWs (or whiskers) during direct vapor deposition has been discussed in early studies [53–55]. However, as depicted in Fig. 6, growth of CuO NWs does not involve direct impingement of Cu ions onto the NW sides (incorporation of oxygen atoms into the NW is not a rate-limiting factor for NW growth because of their easy availability from the vapor). Alternatively, Cu ions are first delivered onto the substrate surface via outward GB diffusion, and a fraction of these Cu ions are incorporated into the substrate oxide and the remaining Cu atoms are transferred onto the NW via adatom–NW exchange by surface diffusion. The density of Cu ions on the substrate surface, n_s, can be described by the following equation:

$$D_s\nabla^2 n_s - n_s/\tau_s + J_{GB} = \frac{\partial n_s}{\partial t} \quad (4)$$

where D_s is the surface diffusivity of Cu ions, J_{GB} is the flux of Cu ions delivered onto the substrate via GB diffusion, and τ_s is the average time a Cu ion diffuses before being incorporated into the oxide phase by reacting with the vapor oxygen. The boundary conditions which apply for diffusion on the substrate are $n_s(r=R) = n_s^R(t)$ and $n_s(r=\infty) = n_s^\infty = J_{GB}\tau_s$, where R is the radius of the NW. With these conditions, the steady-state solution to the substrate diffusion problem is

$$n_s^\infty - n_s(r) = \left[n_s^\infty - n_s^R(t)\right]\frac{K_0(r/\lambda_s)}{K_0(R/\lambda_s)} \quad (5)$$

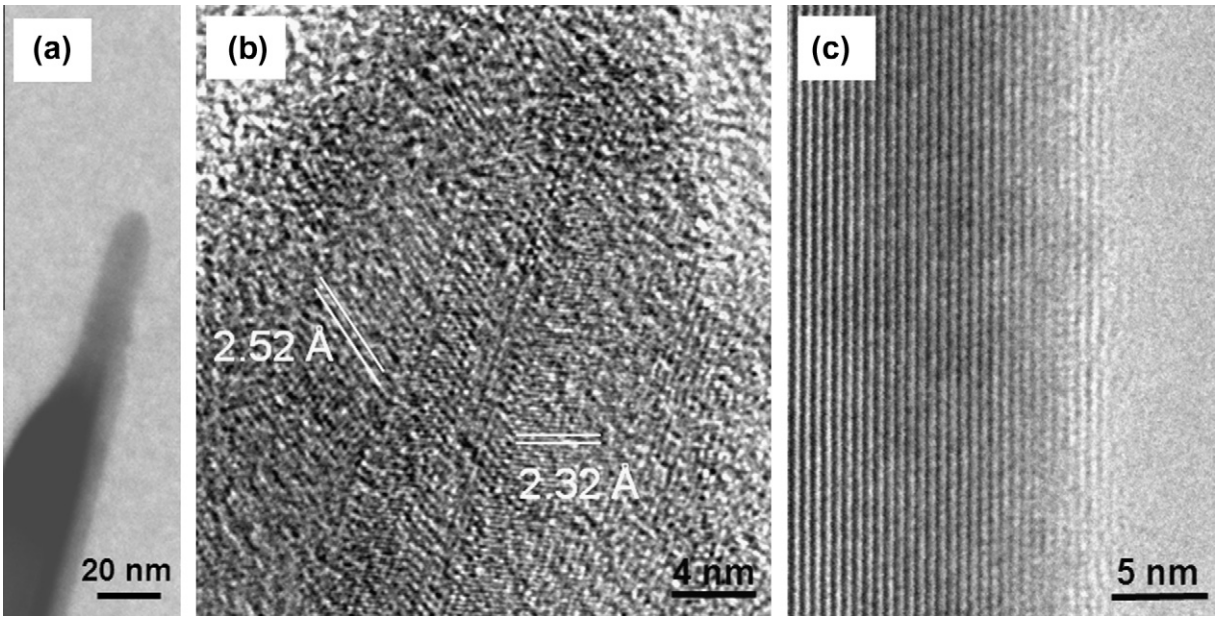

Fig. 7. (a) BF TEM image of the tip of a single CuO NW, (b) HRTEM image showing the presence of atomic steps around the tip, and (c) HRTEM image of the region away from the tip, showing the absence of atomic steps along the NW side surface, where the lattice spacing corresponds to $(2\,0\,\bar{2})$ planes.

where K_0 is the modified Bessel function of the second kind of zero order, and $\lambda_s = (D_s\tau_s)^{1/2}$ is the surface diffusion length on the substrate.

For diffusion of Cu ions on the NW sidewall, we adopt a moving coordinate system whose origin, $z = 0$, is fixed at the tip of the NW [53]. The differential diffusion equation then assumes the form

$$\frac{\partial n_w(z,t)}{\partial t} = D_w\frac{\partial^2 n_w}{\partial z^2} - V\frac{\partial n_w(z,t)}{\partial z} - n_w/\tau_w \tag{6}$$

where z is the length coordinate along the NW, $z = 0$ at the tip, and $z = h$ at the NW base (see Fig. 6), V is the growth rate of the NW, and D_w, and τ_w are the diffusivity and diffusion time of Cu ions on the NW, respectively. The growth rate V can be written as

$$V(t) = \frac{dh(t)}{dt} = \frac{2\Omega D_w}{R}\left[\frac{\partial n_w(z,t)}{\partial z}\right]_{t,z=0}$$

where Ω is the atomic volume of a Cu ion, and R is the radius of the NW. The diffusion on the NW (i.e., Eq. (6)) obeys the boundary conditions of $n_w(z = h) = n_w^h(t)$ at the NW base and $n_w(z = 0) = n_w^0$ at the NW tip, where n_w^h is the concentration of Cu ions at the NW base, and n_w^0 is the concentration of Cu ions at the NW tip in equilibrium with the oxygen gas.

Conservation of mass for exchange of Cu ions between the substrate and the NW sidewall leads to the continuity equations

$$D_w\left[\frac{dn_w(z)}{dz}\right]_{z=h} = D_s\left[\frac{dn_s(r)}{dr}\right]_{r=R} \tag{7}$$

and

$$n_w^h(t) = n_w^R(t)$$

Substituting Eq. (5) into the continuity conditions of Eq. (7), one obtains

$$n_w^h(t) = \left\{\beta n_s^\infty \sinh\left[\frac{h}{\lambda_w}\right] + n_w^0 - n_s^\infty + n_s^\infty \cosh\left[\frac{h}{\lambda_w}\right]\right\} \times \left\{\cosh\left[\frac{h}{\lambda_w}\right] + \beta\sinh\left[\frac{h}{\lambda_w}\right]\right\}^{-1} \tag{8}$$

with the parameters

$$\beta = \left(\frac{\lambda_s}{\lambda_w}\right)\left[\frac{K_1(\sqrt{2}R/\lambda_s)}{K_0(\sqrt{2}R/\lambda_s)}\right] \quad \text{and} \quad \lambda_w = (D_w\tau_w)^{1/2}$$

where K_1 is the modified Bessel function of the second kind of first order and λ_w is the surface diffusion length on the NW. The steady-state solution to Eq. (6) with the substitution for $n_w^h(t)$ from Eq. (8) gives the NW growth law as

$$\frac{dh}{dt} = \frac{\sqrt{2}D_w\Omega(n_s^\infty - n_w^0)}{\lambda_w R}\left[\sinh\left(\frac{h}{\lambda_w}\right) + \beta\cosh\left(\frac{h}{\lambda_w}\right)\right] \times \left[\cosh\left(\frac{h}{\lambda_w}\right) + \beta\sinh\left(\frac{h}{\lambda_w}\right)\right]^{-1} \tag{9}$$

In Eq. (9) the total amount of Cu cations delivered by GB diffusion onto the substrate is given by the term $n_s^\infty = J_{GB}\tau_s$. The NW growth rate depends on the diffusion of Cu ions from the substrate surface (λ_s through β) up along the NW sidewall (λ_w). The integral of the above equation is given by

$$t = \frac{\lambda_w^2 R}{2D_w\Omega(n_z^\infty - n_w^0)}\ln\left[\cosh\left(\frac{h}{\lambda_w}\right) + \beta^{-1}\sinh\left(\frac{h}{\lambda_w}\right)\right] \tag{10}$$

The above equation gives the NW length h as a function of NW diameter during a fixed duration of NW growth for the oxidation at a constant temperature and oxygen

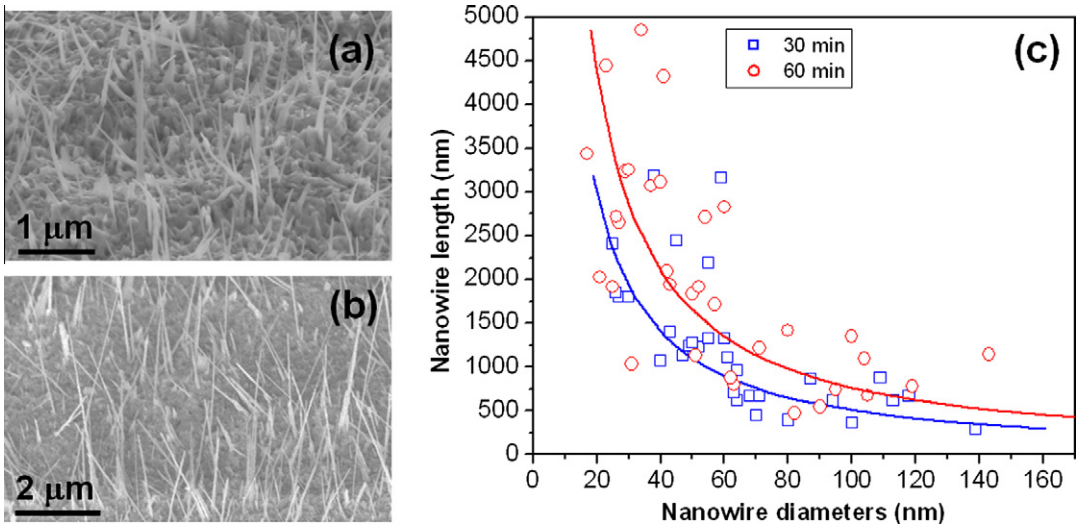

Fig. 8. SEM images of CuO NWs by oxidizing Cu substrates at 350 °C for different oxidation durations: (a) 30 min; (b) 60 min; (c) model (solid curves) fitted to experimental values of the NW length vs. diameter.

pressure. As can be seen from Eq. (10), the NW length h is inversely proportional to the NW radius R for a fixed oxidation time t, i.e. the thinner nanowires are longer than the thicker ones. Fig. 8a and b shows SEM images of CuO NWs formed from the oxidation of Cu substrates at 350 °C and $pO_2 = 50$ torr. Quantitative measurements of NW lengths and radii are conducted on the samples. The experimentally obtained individual NW lengths are plotted vs. the radii in Fig. 8c. The scattered distribution of the experimental data could be ascribed to the fact that not all NWs are nucleated at the same time. The solid curves result from theoretical fitting using Eq. (10), where the fitting parameters are $\frac{2D_w\Omega(n_z^\infty - n_w^0)}{\lambda_w^2} = 2.5\ (\frac{\text{nm}}{\text{min}})$, $\beta^{-1} = 1.5$, and $\lambda_w = 600$ nm. It can be seen that the general trend agrees well between the experimental data and the kinetic model, i.e., thinner NWs are longer than thicker ones. Although D_w cannot be determined from the fitting parameter since n_z^∞ and n_w^0 are unknown, λ_w has a reasonable value for surface diffusion. We see also that the length of NWs increases with the oxidation time. There is, however, a limited oxidation time interval for reliable measurements of the NW length due to the CuO substrate growth effect discussed below.

As noted from the above kinetic model, some Cu cations are incorporated into the substrate before reaching the NW base. Therefore, the CuO substrate will be also growing during the NW growth. This can be evidenced by Fig. 4c, which reveals that the CuO layer grows continuously although the growth rate is very slow. However, for prolonged oxidation and/or higher oxidation temperatures, the growing CuO substrate may gradually bury CuO NWs from their bases and up, as shown schematically in Fig. 9a and b. Since the Cu_2O layer grows via decomposing the CuO layer at the Cu_2O/CuO interface, continued growth of the Cu_2O layer can eventually consume all the CuO phase underneath the CuO NWs, leading to direct contact of CuO NW roots with the Cu_2O layer, as shown

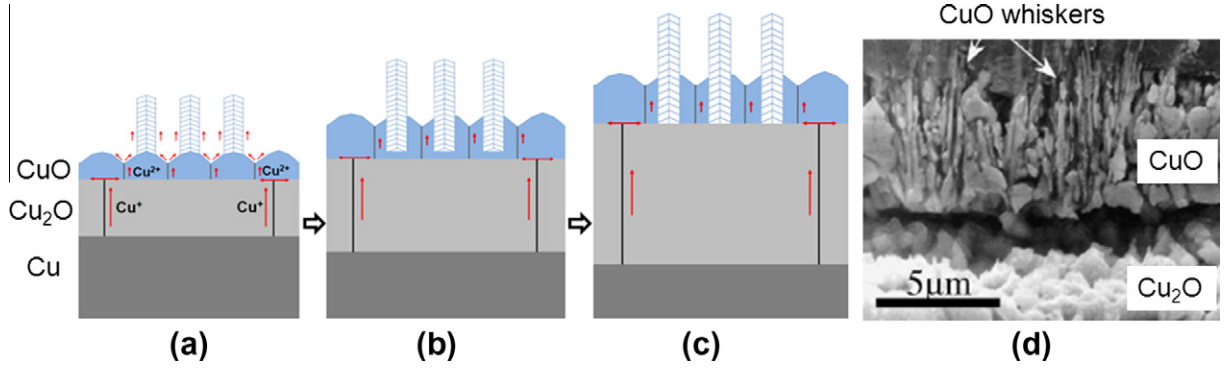

Fig. 9. (a) Initial growth of CuO NWs on the outer surface of CuO grains; (b) growth of the CuO substrate gradually buries the root of the NWs; (c) continued decomposition of the CuO layer at the CuO/Cu_2O interface leading to the direct contact between the NW roots and the Cu_2O layer; (d) an experimental cross-sectional SEM image from the oxidation of Cu at 600 °C for 4 h, showing that CuO whiskers are buried by the CuO layer and their roots have direct contact with the Cu_2O layer [56].

in Fig. 9c. This mechanism involving the two simultaneous processes, i.e., burying oxide NWs by the growing CuO substrate and decomposing the CuO substrate at the CuO/Cu_2O interface, reconciles our results with previous studies, which showed that CuO whiskers are directly in contact with the CuO/Cu_2O interface [19,30,56]. Fig. 9d shows an example of cross-sectional SEM images reported by Zhu et al., where the Cu substrate was oxidized at 600 °C for 4 h [30,56]. It can be seen from the SEM image that CuO whiskers are buried by the CuO layer and the NW roots are close to the CuO/Cu_2O (i.e., corresponding to the situation of Fig. 9b).

It was shown previously that oxidation temperature can significantly affect the reaction product and morphology, and CuO NW formation occurs mainly within a temperature window from ~250 °C to 700 °C [8,13,17,19,21–23,57]. Since the growth of oxide NWs requires effective GB diffusion driven by the compressive stress. For oxidation at low temperature (<250 °C), the CuO/Cu_2O interface reaction is slow due to the low mobility of Cu cations and vacancies. Therefore, the rate of stress generation by the solid-state phase transformation is not sufficient to activate effective GB diffusion for oxide NW growth. On the contrary, as the temperature is increased to over 700 °C, lattice diffusion becomes more favorable than GB diffusion. The interface strain associated with the phase transformation at the CuO/Cu_2O interface can be released quickly by fast lattice diffusion, leading to uniform growth of CuO grains. In addition, oxide growth facilitated by the enhanced lateral lattice diffusion can also cause flatter morphologies at the high temperatures. Thus, oxide NW growth is observed only in the immediate oxidation temperature regime which promotes oxide NW growth via effective GB diffusion through the thin CuO layer.

5. Conclusions

We present a detailed study on the growth of CuO NWs by thermal oxidation of Cu substrates. The occurrence of CuO NW is identified by atom diffusion rather than mechanical flow. The interfacial strain associated with the solid-state phase transformation at the CuO/Cu_2O interface drives outward grain-boundary diffusion of cations, which acts as a continual source of Cu ions for CuO NW growth on CuO grains. The formation of twin boundaries in NWs is attributed to the surface faceting of CuO grains which serve as the template for initiating the nucleation and growth of CuO NWs. CuO NWs grow at their tip, where atomic steps around the tip provide sites for easy attachment for Cu cations supplied by the substrate–NW adatom exchange via surface diffusion.

Acknowledgements

We acknowledge support from the National Science Foundation under Grant No. CMMI-0825737. The sample fabrication work was funded by the Department of Energy Grant No. DE-FG02-09ER46600. Y.Q. Wang would like to thank the financial support from the Natural Science Foundation for Outstanding Young Scientists in Shangdong Province, China (Grant No. JQ201002).

References

[1] Comini E, Baratto C, Faglia G, Ferroni M, Vomiero A, Sberveglieri S. Prog Mater Sci 2009;54:1.
[2] Sun YH, Gao JY, Zhu R, Xu J, Chen L, Zhang JM, et al. J Chem Phys 2010;132:124705.
[3] Nasibulin AG, Rackauskas S, Jiang H, Tian Y, Mudimela PR, Shandakov SD, et al. Nano Res 2009;2:373.
[4] Wang RM, Chen YF, Fu YY, Zhang H, Kisielowski C. J Phys Chem B 2005;109:12245.
[5] Wen XG, Wang SH, Ding Y, Wang ZL, Yang SH. J Phys Chem B 2005;109:215.
[6] Liao L, Zhang Z, Yan B, Zheng Z, Bao QL, Wu T, et al. Nanotechnology 2009;20:085203.
[7] Fu YY, Chen J, Zhang J. Chem Phys Lett 2001;350:491.
[8] Jiang XC, Herricks T, Xia YN. Nano Lett 2002;2:1333.
[9] Zhong ML, Zeng DC, Liu ZW, Yu HY, Zhong XC, Qiu WQ. Acta Mater 2010;58:5926.
[10] Arnold SM, Koonce SE. J Appl Phys 1956;27:964.
[11] Sartell JA, Stokes RJ, Bendel SH, Johnson TL, Li CH. Trans Metall Soc AIME 1959;215:420.
[12] Hsieh CT, Chen JM, Lin HH, Shih HC. Appl Phys Lett 2003;82:3316.
[13] Huang LS, Yang SG, Li T, Gu BX, Du YW, Lu YN, et al. J Cryst Growth 2004;260:130.
[14] Kofstad P. High temperature corrosion. New York: Elsevier Applied Science; 1988.
[15] Rapp RA. Metall Trans B 1983;15B:195.
[16] Rapp RA. Metall Mater Trans A 1984;15A:765.
[17] Raynaud GM, Rapp RA. Oxid Metals 1984;21:89.
[18] Voss DA, Bulter EP, Michell TE. Metall Trans A 1982;13A:929.
[19] Goncalves AM, Campos LC, Ferlauto AS, Lacerda RG. J Appl Phys 2009;106:034303.
[20] Kumar A, Srivastava AK, Tiwari P, Nandedkar RV. J Phys: Condens Matter 2004;16:8531.
[21] Chen JT, Zhang F, Wang J, Zhang GA, Miao BB, Fan XY, et al. J Alloys Compd 2008;454:268.
[22] Xu CH, Woo CH, Shi SQ. Chem Phys Lett 2004;399:62.
[23] Kaur M, Muthe KP, Despande SK, Choudhury S, Singh JB, Verma N, et al. J Cryst Growth 2006;289:570.
[24] Zhang K, Rossl C, Tenalleau C, Alphonse P, Chane-Ching JY. Nanotechnology 2007;19:275607.
[25] Chopra N, Hu B, Hinds B. J Mater Res 2007;22:2691.
[26] Appleby WK, Tylecote RF. Corros Sci 1970;10:325.
[27] Morin F. J Mater Sci Lett 1983;2:383.
[28] Evans HE. Int J Mater Res 1995;40:1.
[29] Zhu Y, Mimura K, Isshiki M. Oxid Metals 2004;62:207.
[30] Zhu YF, Mimura K, Isshiki M. Mater Trans 2002;43:2173.
[31] Grzesik Z, Migdalska M. Def Diffus Forum 2009;289–292:429.
[32] Zhu YF, Mimura K, Lim JW, Isshiki M, Jiang Q. Metall Mater Trans A 2006;37A:1231.
[33] Komatsu M, Mori H. J Electron Microsc 2005;54:99.
[34] Musa AO, Akomolafe T, Carter MJ. Solar Energy Mater Solar Cells 1998;51:305.
[35] Fernando CAN, de Silva PHC, Wethasinha SK, Dharmadasa IM, Delsol T, Simmonds MC. Renew Energy 2002;26:521.
[36] Siripala W, Ivanovskaya A, Jaramillo TF, Baeck SH, McFarland EW. Solar Energy Mater Solar Cells 2003;77:229.
[37] Zhou L, Gunther S, Moszynski D, Imbihl R. J Catal 2005;235:359.
[38] Wang XQ, Rodriguez JA, Hanson JC, Gamarra D, Martinez-Arias A, Fernandez-Garcia M. J Phys Chem B 2005;109:19595.
[39] Wang JB, Tsai DH, Huang TJ. J Catal 2002;208:370.

[40] Liu W, Flytzani-stephanopoulos M. J Catal 1995;153:317.
[41] Wang XQ, Hanson JC, Frenkel AI, Kim JY, Rodriguez JA. J Phys Chem B 2004;108:13667.
[42] Poizot P, Laruelle S, Grugeon S, Dupont L, Tarascon JM. Nature 2000;407:496.
[43] Shishiyanu ST, Shishiyanu TS, Lupan OL. Sens Actuat B: Chem 2006;113:468.
[44] Pradhan S, Reddy AS, Devi RN, Chilukuri S. Catal Today 2009;141:72.
[45] Horne A, Hungria AB, Bera P, Camara AL, Fernandez-Garcia M, Martinez-Arias A, et al. J Am Chem Soc 2010;132:34.
[46] Barsoun MW, Hoffman EN, Doherty RD, Gupta S, Zavaliangos A. Phys Rev Lett 2004;93:206104.
[47] Avramov I. Nanoscale Res Lett 2007;2:235.
[48] Fromhold AT, Fromhold RG. In: Bamford CH, Tipper CFH, Compton RG, editors. Reactions of solids with gases, vol. 21. New York: Elsevier; 1984.
[49] Nikolay JR, Dmitry VY, Chicherin DS, Tretyakov YD, Leonyuk LI, Yakunin VG. J Mater Chem 1997;7:2085.
[50] Peterson NL, Wiley CL. J Phys Chem Solids 1984;45:281.
[51] Cooks AFC. In: Allison IM, Ruiz C, editors. Applied solid mechanics. Amsterdam: North Holland; 1989. p. 30.
[52] Burton WK, Cabrera N, Frank FC. Philos Trans Roy Soc London A 1951;243:299.
[53] Ruth V, Hirth JP. J Chem Phys 1964;41:3139.
[54] Johansson J, Svensson CPT, Martensson T, Samuelson L, Seifert W. J Phys Chem B 2005;109:13567.
[55] Dayeh SA, Yu ET, Wang DL. Nano Lett 2009;9:1967.
[56] Zhu YF, Mimura K, Isshiki M. Corros Sci 2005;47:537.
[57] Onay B, Rapp RA. Oxid Metals 1988;29:473.